Simulating water hammer with corrective smoothed particle method

EINDHOVEN UNIVERSITY OF TECHNOLOGY
Department of Mathematics and Computer Science

CASA-Report 12-14
May 2012

Simulating water hammer with corrective smoothed particle method

by

Q. Hou, A.C.H. Kruisbrink, A.S. Tijsseling, A. Keramat

Centre for Analysis, Scientific computing and Applications
Department of Mathematics and Computer Science
Eindhoven University of Technology
P.O. Box 513
5600 MB Eindhoven, The Netherlands
ISSN: 0926-4507

Simulating water hammer with corrective smoothed particle method

Q. Hou[1], *A.C.H. Kruisbrink*[2], *A.S. Tijsseling*[1], *A. Keramat*[3]
[1] *Eindhoven University of Technology, The Netherlands*
[2] *The University of Nottingham, United Kingdom*
[3] *Jundi Shapur University of Technology, Iran*

ABSTRACT

The corrective smoothed particle method (CSPM) is used to simulate water hammer. The spatial derivatives in the water-hammer equations are approximated by a corrective kernel estimate. For the temporal derivatives, the Euler-forward time integration algorithm is employed. The CSPM results are in good agreement with solutions obtained by the method of characteristics (MOC). A parametric study gives insight in the effects of particle distribution, smoothing length and kernel function. Three typical water-hammer problems are solved. CSPM will not beat MOC in classical water-hammer, but it has potential for water-hammer problems with free surfaces as seen in column separation and slug impact.

1 INTRODUCTION

Transient flow in piping systems is generally caused by rapid changes in flow conditions due to sudden valve operation, pump start up or shut down, power failure, etc. The phenomenon is generally called pressure surge or water hammer, and it may damage hydraulic machinery, piping and supports. If possible, it should be anticipated in the design process and prevented in practice. For details on transient flow, see the widely used textbook by Wylie *et al.* [1].

For the simulation of transient flows in pipes, several methods are available. Before the digital computer era, graphical techniques were used. The accuracy of this method can be low, since friction is not properly taken into account. The solution procedure can be very elaborate and is rarely used nowadays. For details on the graphical method, interested readers are referred to the summary by Lupton [2]. Nowadays, the most commonly used approach is the computerized method of characteristics (MOC), which has been employed numerically to simulate transient flow in complex pipe systems since the mid 1960s. Later, water-hammer models were extended with associated phenomena such as gas release, column separation, unsteady friction, pipe wall viscoelasticity and fluid-structure interaction. Details on MOC and its practice can be found in [1] and the recent review papers [3, 4]. Other methods for the numerical solution of the transient flow equations include the explicit [5] and implicit [6, 7, 8, 9] finite-difference method (FDM), the finite-element method (FEM) [10, 11], Godunov method [12, 13], lattice-Boltzmann method (LBM) [14, 15] and an explicit central-difference scheme with total variational diminishing (TVD) [16]. A direct finite-difference methodology was described in [17], but no results were presented.

In the present paper, the corrective smoothed particle method (CSPM) is used to simulate transient flow in a reservoir-pipe-valve system. In the CSPM particle

method for the water-hammer problem, the spatial derivatives are approximated using corrective kernel estimates. For an acceptable accuracy and high computational efficiency, the temporal derivatives are integrated by the Euler-forward method. To prevent numerical oscillations, an artificial dissipative term is added to the momentum equation. This artificial viscosity term is switched on in regions of high velocity gradients and switched off in smooth regions by evaluating the gradient of the particle velocity. The main effects of several key factors on the performance of CSPM are investigated. These factors are the particle distribution (evenly and randomly spaced), artificial viscosity, the kernel or smoothing function, smoothing length, pre-smoothing and number of particles.

CSPM is for the first time successfully applied to weakly compressible flow. Water hammer is chosen as a test problem of practical importance, since it has a validated solution, which is used as a reference. CSPM has been selected because it has potential for simulating water-hammer events that involve free surfaces, cavitation, liquid slugs and fluid-structure interaction [18, 19]. Water-hammer problems including instantaneous and gradual valve closure, line pack and column separation are solved herein.

2 MATHEMATICAL MODELLING

2.1 Governing equations

The governing equations for one-dimensional single-phase transient flow in pipes comprise the following continuity and momentum equations in Eulerian form [1]

$$\frac{\partial P}{\partial t}+\left[V\frac{\partial P}{\partial x}\right]+\rho c^2\frac{\partial V}{\partial x}=0, \quad \frac{\partial V}{\partial t}+\left[V\frac{\partial V}{\partial x}\right]+\frac{1}{\rho}\frac{\partial P}{\partial x}+g\frac{\mathrm{d}z}{\mathrm{d}x}+\frac{\lambda V|V|}{2D}=0, \quad (1)$$

where P is the pressure, V is the mean flow velocity, ρ is the fluid density, c is the sonic wave speed, g is the gravitational acceleration, t and x denote the time and the axial distance along the pipe, z is the pipe elevation, D is the inner pipe diameter, and λ is the Darcy-Weisbach friction factor. Note that the convection terms between square brackets are usually neglected under the assumption that $V << c$. The liquid compressibility, pipe elasticity and wall constraint conditions are included in the model through the expression for wave speed

$$c:=\sqrt{\frac{K}{\rho}\left(1+\phi\frac{DK}{Ee}\right)^{-1}}, \quad (2)$$

in which K is the bulk modulus of the fluid, e is the pipe wall thickness, ϕ denotes the structural constraint condition of the pipe, for which typical values are given in [1]. For a pipe, which is free at one end and supplied with expansion joints at regular intervals along its length, the coefficient ϕ is unity.

2.2 Modified momentum equation

For the solution of hyperbolic equations, a dissipative term is usually needed to suppress numerical wiggles. Numerical damping can be introduced explicitly [5, 16] or implicitly [6, 7, 8, 9, 12, 13] in regions of high gradients. For the fast transient flow investigated herein, an explicit dissipative term is added to the momentum equation, which is called artificial viscosity in smoothed particle hydrodynamics (SPH) [20]. After adding the dissipation term in the momentum

equation, and with constant z and material derivatives, from (1) we get

$$\frac{\mathrm{D}P}{\mathrm{D}t} = -\rho c^2 \frac{\partial V}{\partial x}, \qquad \frac{\mathrm{D}V}{\mathrm{D}t} = -\frac{1}{\rho}\frac{\partial P}{\partial x} - \frac{\lambda V|V|}{2D} + \frac{\partial(\rho\Pi)}{\partial x}. \tag{3}$$

This Lagrangian form of the continuity and momentum equations will be solved with CSPM, as described in Section 4.

3 THE METHOD OF CHARACTERISTICS

The method of characteristics (MOC) is established in the numerical simulation of transient flow in pipelines. It is briefly described in this section. The governing equations of transient flow form a pair of quasi-linear hyperbolic partial differential equations (PDEs). They can be transformed via the MOC into a pair of ordinary differential equations (ODEs) and then solved by numerical integration. Solving (1) by the MOC for constant z leads to the following so-called compatibility and characteristic equations

$$\frac{\mathrm{d}V}{\mathrm{d}t} \pm \frac{1}{\rho c}\frac{\mathrm{d}P}{\mathrm{d}t} + \frac{\lambda V|V|}{2D} = 0, \qquad \frac{\mathrm{d}x}{\mathrm{d}t} = [V] \pm c. \tag{4}$$

The solution of these equations is used as the reference solution in Section 5.

4 CORRECTIVE SMOOTHED PARTICLE METHOD

The corrective smoothed particle method (CSPM), proposed by Chen *et al.* [21, 22], is a generalization of standard SPH [23]. The key idea of CSPM is to expand the kernel estimate, an essential element in SPH, into a Taylor series. Compared with other modifications to SPH, the CSPM algorithm is quite straightforward [21]. It not only remedies the two drawbacks in SPH, namely boundary deficiency [21] and tensile instability [22], but also extends the ability of SPH in solving PDEs containing second-order derivatives. The two essential components of CSPM, the corrective kernel estimate and the particle approximation, are described in this section. Since transient flow in pipes is modelled herein as a one-dimensional problem, only those formulations that are required in the current work are presented. For the basic theory of CSPM in multi-space dimensions, see e.g. [21, 22].

4.1 Corrective kernel approximation

Expanding a smooth function $f(x)$ in the neighbourhood of point x_i into a Taylor series, multiplying both sides of the expansion by a smoothing function or kernel, and integrating over the one-dimensional domain Ω yields

$$\begin{aligned}\int_\Omega f(x)W_i(x)dx =& f(x_i)\int_\Omega W_i(x)dx + f_x(x_i)\int_\Omega (x-x_i)W_i(x)dx \\ &+ \frac{1}{2}f_{xx}(x_i)\int_\Omega (x-x_i)^2 W_i(x)dx + \cdots,\end{aligned} \tag{5}$$

where $f_x := df/dx$, $f_{xx} := d^2f/dx^2$ and $W_i(x) := W(x - x_i, h_i)$ is the kernel associated with point x_i. The influence of the kernel is limited to a support proportional to the smoothing length h_i. The influence domain of point x_i is the region where $W(x - x_i, h_i) > 0$.

Neglecting all the derivative terms in (5) gives the corrective kernel estimate of the function $f(x)$ at point x_i,

$$\hat{f}(x_i) := \frac{\int_\Omega f(x) W_i(x) \mathrm{d}x}{\int_\Omega W_i(x) \mathrm{d}x}. \tag{6}$$

The hat symbol denotes an approximation throughout this work. For a symmetric kernel, the second term at the right-hand side (RHS) of (5) vanishes for interior regions, but does not so for boundary regions because of a truncated support. The corrective kernel estimate of the function expressed in (6) is therefore of order h_i^2 accuracy for points x_i far away from the boundary, and of order h_i for points x_i near or on the boundary.

If the kernel $W_i(x)$ in (5) is replaced by its derivative $W_{i,x} := \mathrm{d}W_i(x)/\mathrm{d}x$ and the second and higher derivative terms are neglected, a corrective kernel estimate of the first-derivative $f_x(x)$ is generated as

$$\hat{f}_x(x_i) := \frac{\int_\Omega [f(x) - f(x_i)] W_{i,x} \mathrm{d}x}{\int_\Omega (x - x_i) W_{i,x} \mathrm{d}x}. \tag{7}$$

The CSPM kernel estimate of the first derivative is also second-order accurate for the interior points and first-order accurate for the points near or on the boundary [21]. The derivative of the kernel must be anti-symmetric to avoid a zero denominator in (7).

4.2 Particle approximation

Taking care that the spatial domain is represented by particles, formulas (6) and (7) are integrated per particle volume. This results in a weighted volume summation over the particles. If the particle volume is replaced by its mass to density ratio, the so-called particle approximations become

$$\hat{f}_i := \frac{\sum_{j=1}^{N} f_j W_{ij}\ m_j/\rho_j}{\sum_{j=1}^{N} W_{ij}\ m_j/\rho_j} = \frac{\sum_{j\in S_i} f_j W_{ij}\ m_j/\rho_j}{\sum_{j\in S_i} W_{ij}\ m_j/\rho_j}, \tag{8}$$

$$\hat{f}_{i,x} := \frac{\sum_{j=1}^{N} (f_j - f_i) W_{ij,x}\ m_j/\rho_j}{\sum_{j=1}^{N} (x_j - x_i) W_{ij,x}\ m_j/\rho_j} = \frac{\sum_{j\in S_i} (f_j - f_i) W_{ij,x}\ m_j/\rho_j}{\sum_{j\in S_i} (x_j - x_i) W_{ij,x}\ m_j/\rho_j}. \tag{9}$$

in which $f_i := f(x_i)$, $f_j := f(x_j)$, $W_{ij} := W(x_j - x_i, h)$, $f_{i,x} := f_x(x_i)$ and $W_{ij,x} := W_{i,x}(x_j)$, N is the total number of particles in the domain, and m_j and ρ_j are the mass and density of particle j, respectively. The kernel associated with particle i has a compact support that is much smaller than Ω, so that the number of particles within the summations is actually much smaller than N. Suppose that there are N_i particles in the support of W_i forming the set S_i, then we get the last terms in (8) and (9).

Particle i and the other particles in the support of $W_i(x)$ constitute so-called interaction pairs. A particle search needs to be executed to find S_i and thus the interaction pairs ahead of any calculation [20]. Compared with the conventional kernel estimate of the function $f(x)$ in SPH, i.e. $\hat{f}_i := \sum_{j\in S_i} f_j W_{ij}\ m_j/\rho_j$, the denominator in (8) is the essential correction for the boundary deficiency [21]. To avoid (9) becoming singular, at least one other particle should be within the influence domain of particle i. The smoothing length h_i has to be within a certain range to meet this requirement. This is in particular important for particles in the boundary region, because their support is truncated.

4.3 Kernel

A common choice of the kernel is the cubic spline function

$$W(q,h) := \frac{1}{h}\begin{cases} 2/3 - q^2 + q^3/2, & 0 \leqslant q < 1, \\ (2-q)^3/6, & 1 \leqslant q < 2, \\ 0, & q \geqslant 2, \end{cases} \tag{10}$$

where q is the distance between two particles scaled by the smoothing length, i.e. $q := |x - x_i|/h$. The cubic spline function and its first derivative are shown in Fig. 1. The kernel W is symmetric and its derivative is anti-symmetric.

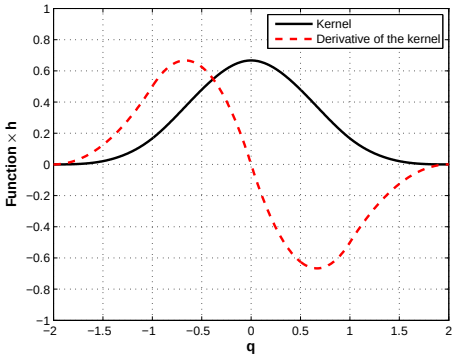

Figure 1: **Cubic spline function and its derivative.**

4.4 Time-integration algorithm

Meshfree particle methods transform PDEs into ODEs in time. To solve these ODEs, a proper time-integration algorithm is needed. A large variety of time integration methods is available and any choice will be a compromise between accuracy, computational efficiency and robustness.

For a set of n coupled first-order differential equations of the form

$$\mathrm{d}\mathbf{y}/\mathrm{d}t = F(\mathbf{y}, t), \ \mathbf{y} \in \mathbb{R}^n, \tag{11}$$

the evaluation of $F(\mathbf{y}, t)$ usually dominates the computational effort. Consequently, for efficiency, the number of evaluations within each time step should be kept as small as possible. The term is evaluated only once in the Euler forward method, whereas it is evaluated at least twice in other explicit time-integration methods such as modified Euler, Runga-Kutta and leapfrog [24]. Therefore, the conditionally stable Euler forward method is employed in this paper for time marching. This time-integration algorithm has first-order accuracy.

The solution is advanced from t^n to t^{n+1} according to

$$P_i^{n+1} = P_i^n + \Delta t \left(\frac{\mathrm{D}P}{\mathrm{D}t}\right)_i^n, \qquad V_i^{n+1} = V_i^n + \Delta t \left(\frac{\mathrm{D}V}{\mathrm{D}t}\right)_i^n, \tag{12}$$

where the superscripts indicate the time level, and the total time derivatives are obtained from (3) as

$$\left(\frac{\mathrm{D}P}{\mathrm{D}t}\right)_i^n = -\rho c^2 \left(\frac{\partial V}{\partial x}\right)_i^n, \quad \left(\frac{\mathrm{D}V}{\mathrm{D}t}\right)_i^n = -\frac{1}{\rho}\left(\frac{\partial P}{\partial x}\right)_i^n - \frac{\lambda V_i^n |V_i^n|}{2D} + \left(\frac{\partial(\rho\Pi)}{\partial x}\right)_i^n. \tag{13}$$

The spatial derivatives $(\partial V/\partial x)_i^n$ and $(\partial P/\partial x)_i^n$ in (13) are approximated using formula (9) by substituting P and V for f. For the nonlinear friction term, the velocities at the previous time step are used. The flow chart of the solution procedure is given in the Appendix. The approximation of the artificial dissipation term $(\partial(\rho\Pi)/\partial x)_i^n$ is less straightforward and is discussed below.

4.5 Artificial viscosity

In this paper, the dissipation term $(\partial(\rho\Pi)/\partial x)_i^n$ is modelled as an artificial viscosity [25] for the SPH simulation of shock waves,

$$\left(\frac{\partial(\rho\Pi)}{\partial x}\right)_i = \sum_{j\in S_i} m_j \Pi_{ij} W_{ij,x}, \tag{14}$$

$$\Pi_{ij} := \begin{cases} \dfrac{-\alpha c \mu_{ij} + \beta \mu_{ij}^2}{\rho}, & (V_i - V_j)(x_i - x_j) < 0, \\ 0, & (V_i - V_j)(x_i - x_j) \geqslant 0, \end{cases} \tag{15}$$

$$\mu_{ij} := \frac{\bar{h}_{ij}(V_i - V_j)(x_i - x_j)}{|x_i - x_j|^2 + \eta \bar{h}_{ij}^2}, \tag{16}$$

where α, β and η are constant coefficients, and $\bar{h}_{ij} := (h_i + h_j)/2$ is the average of the smoothing lengths associated to particle i and particle j. The linear (in velocity difference) term in Π_{ij} produces a shear and a bulk viscosity, while the quadratic term is equivalent to the von Neumann-Richtmyer viscosity [20]. The term $\eta\bar{h}_{ij}^2$ in μ_{ij} is added to prevent a singularity (for $i = j$). Herein, $\alpha = 1$, $\beta = 2$ and $\eta = 0.01$ are used, which are typically values for shocks [20].

4.6 Particle distribution and boundary particles

In this paper, evenly and irregularly spaced particles are considered. For evenly spaced particles, four particle distribution patterns often used in SPH are shown in Fig. 2.

- The cell-centered particle distribution (Fig. 2a) is widely used in SPH. However, the Dirichlet boundary condition cannot be imposed exactly, because the boundary particles do not lie on the physical boundaries.
- The cell-centered particle distribution with virtual particles (Fig. 2b) allows for an exact enforcement of Dirichlet boundary conditions. The total volume is overestimated because two virtual particles are added.
- The vertex-centered particle distribution (Fig. 2c) allows for the same treatment of interior and boundary particles. The enforcement of Dirichlet boundary conditions is also exact. The total volume is slightly overestimated.
- The semi-vertex-centered particle distribution (Fig. 2d) also allows for an exact enforcement of Dirichlet boundary conditions. The total volume is correct, but the treatment of the particles adjacent to the boundary is slightly different, because the boundary particles have a reduced (50%) volume.

The irregularly spaced interior particles used herein are randomly distributed. The following rule is applied to obtain the particle positions

$$x_i = \begin{cases} 0, & i = 1, \\ (i-1)\ \Delta x + R_i\ \zeta\ \Delta x, & i = 2, \cdots, N-1, \\ L, & i = N, \end{cases} \tag{17}$$

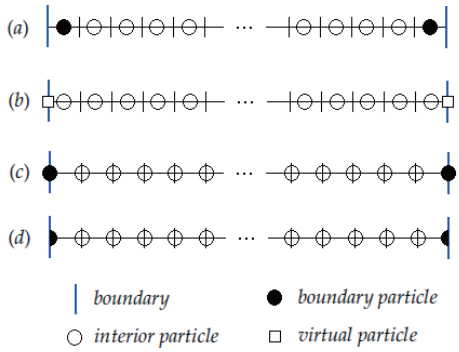

Figure 2: **Evenly spaced particles: (a) cell-centered, (b) cell-centered with virtual boundary particles, (c) vertex-centered, (d) semi-vertex-centered**.

where $\Delta x = L/(N-1)$ is the cell size, L is the domain size, $R_i \in (-0.5, 0.5)$ is a random number and $\zeta \in [0,1]$ is a parameter determining the magnitude of deviations from the vertex centres. This parameter mimics the physical state of particles (solid $\zeta \approx 0$, gas $\zeta \approx 1$). For the weakly compressible liquid in the semi-closed system in Fig. 2, $\zeta = 0.25$ is used. The above particle distributions are examined in Subsection 5.1.

4.7 Boundary and initial conditions

For the waterhammer considered herein, the two boundary conditions are the prescribed velocity at the valve, i.e. $V = 0$ at $x = L$, and the constant pressure at the reservoir, i.e. $P = P_{res}$ at $x = 0$. For most of the meshfree methods, in particular those based on weak forms, special attention needs to be paid to the enforcement of Neumann boundary conditions [26]. However, imposing boundary conditions in CSPM is simple and straightforward. During the solution course, the velocity boundary condition is directly included in the velocity gradient in (13) for the particle at the valve and the particles interacting with it. The same holds for the enforcement of the pressure boundary condition on the particles near the reservoir. The initial condition is given pressure and velocity.

5 SIMULATIONS AND PARAMETRIC CSPM STUDY

CSPM results are presented for a reservoir-pipe-valve configuration (Fig. 3), subjected to instantaneous valve closure, and compared to MOC solutions. The particles are assumed not to move after valve closure, because water hammer is an acoustic phenomenon where all displacements $V \cdot t_w << L$ due to $t_w = L/c$ and $V << c$. The data used in the numerical calculations are for a water-filled steel pipe [27]: $L = 20$ m, $D = 797$ mm, $e = 8$ mm, $E = 210$ GPa, $K = 2.1$ GPa, $\rho = 1000$ kg/m^3, $\phi = 1$, $Q_0 = AV_0 = 0.5$ m^3/s, $P_{res} = 1$ MPa and $\lambda = 0.02$. The wave speed calculated from (2) is 1025.7 m/s. The pipe length is divided into 200 equal parts and the time increment $\Delta t = \Delta x/c = 9.75 \times 10^{-5}$ s, so the Courant number $Cr = c\Delta t/\Delta x = 1$. The simulation time is 0.3 seconds. Since the cell size is $\Delta x = 0.1$ m and the density is assumed to be constant, the particle mass is $\bar{m} = \rho A \Delta x = 49.9$ kg.

We first employ the vertex-centered particle distribution (Fig. 2c), which is used as a reference case. The effect of other distributions, artificial viscosity, presmoothing, smoothing length, number of particles and kernel function, is studied

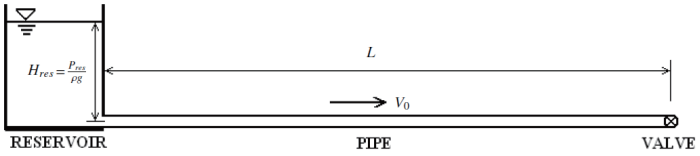

Figure 3: **Schematic of a reservoir-pipe-valve system.**

in the Subsections 5.1 through 5.6. The reference case is a frictionless simulation, i.e. $\lambda = 0$, which is a good and extreme test to identify numerical dissipation and dispersion. The smoothing length is $h_i = \Delta x$, $(i = 1, \cdots, 201)$. Comparisons between the CSPM and MOC solutions are presented in Fig. 4. The CSPM results agree well with the MOC solution. The numerical dispersion is eliminated by artificial viscosity. The usual phase errors (unphysical oscillations or wiggles) and amplitude errors (smearing effect) are largely absent here. Consequently, sharp wave fronts are maintained. An overshoot is visible at the first pressure wave front only, and not in the time history of the upstream velocity. The overshoot is about 6 percent of the pressure variation, and it is treated in Subsection 5.3.

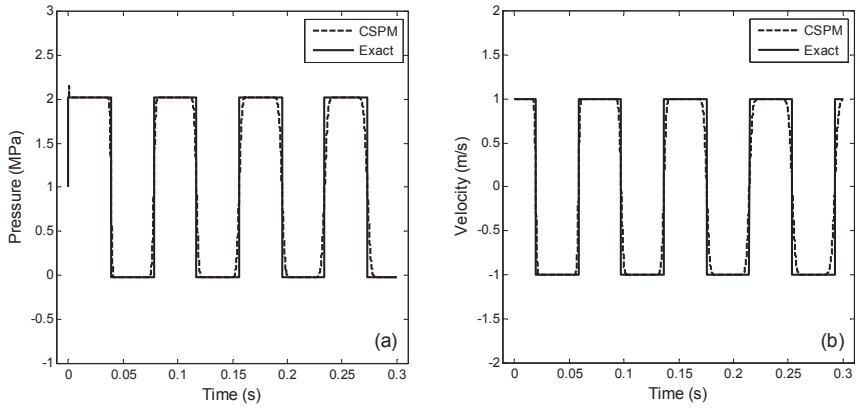

Figure 4: **Time history of the (a) downstream pressure and (b) upstream velocity.**

5.1 Particle distribution

This section demonstrates the effect of particle distributions on the numerical results, and suggests the proper distribution to be used in CSPM simulations.

5.1.1 Evenly spaced particles

Evenly spaced particle distributions are the most used in CSPM [21, 22, 28] and related methods [20, 26, 29]. Since the cell-centered particle distribution in Fig. 2a does not allow exact enforcement of Dirichlet boundary conditions, the other two types shown in Figs. 2b and 2d are examined.

For the particle distribution in Fig. 2b, the virtual boundary particles have the same mass as the interior particles, because the same volume and constant density are assumed. Consequently, we have 202 particles with the same mass $\bar{m}$, so that the total mass of the system is overestimated (if the virtual particles are included in the system) because $202\bar{m} > \rho AL = 200\bar{m}$. The smoothing lengths are taken as Δx, so that each interior particle has two neighbours. For the particle distribution in Fig. 2d, the particle masses are $m_1 = m_{201} = \bar{m}/2$

and $m_i = \bar{m}$ $(i = 2, \cdots, 200)$, so that the total mass is 200 $\bar{m}$. The smoothing lengths are $h_1 = h_{201} = \Delta x/2$ and $h_i = \Delta x$ $(i = 2, \cdots, 200)$.

The results obtained for the three particle distributions in Fig. 5 are nearly the same. The difference is mainly at the first wave front. The details in Fig. 6 show that the vertex-centered particle distribution generates the smallest overshoot. Other simulations, in which the mass of the virtual particles (Fig. 2b) is $m_1 = m_{201} = \bar{m}/2$ and the smoothing length is $h_1 = h_{201} = \Delta x$, were also run. Although all the results were in good agreement with the MOC solution, the vertex-centered particle distribution performed the best.

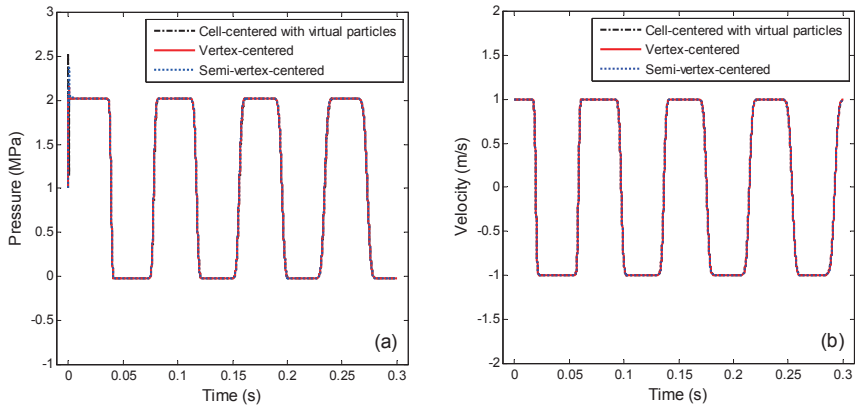

Figure 5: **Effect of evenly spaced particles on the (a) downstream pressure and (b) upstream velocity.**

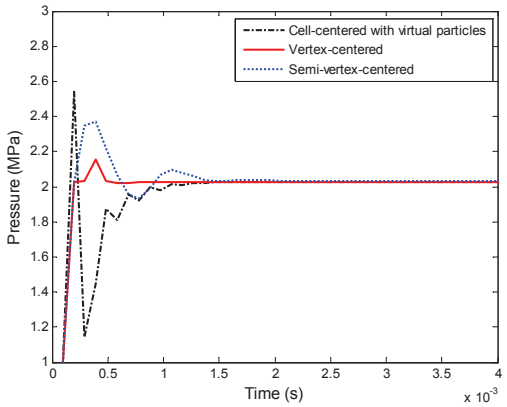

Figure 6: **Same results as shown in Fig. 5, but now on a finer scale to show the details at the first wave front.**

5.1.2 Randomly spaced particles

Randomly spaced particles mimic the meshless situation where the particles go with the flow. They allow for different ways to determine the particle mass and smoothing length. Here we examine three of them. First, we consider constant mass and smoothing length. This is averaging – in a sense – and widely used in SPH [23]. Second, the interior particle mass varies according to $m_i = \rho A(x_i - x_{i-1})$, while at the boundaries $m_1 = m_{201} = \bar{m}$. The smoothing length varies according to $h_i = x_i - x_{i-1}$ $(i = 2, \cdots, 200)$ and $h_1 = h_{201} = \Delta x$. Third,

the interior particle mass is computed from $m_i = \frac{1}{2}\rho A(x_{i+1} - x_{i-1})$, and at the boundaries $m_1 = m_{201} = \bar{m}$. For all particles, the smoothing length is taken as the maximum distance between two neighbours. We denote these three different approaches as RA1 (random approach 1), RA2 and RA3. The results in Fig. 7 show that all three cases give reasonable solutions, but not more than that. The results of RA3 are the best, and closest to those in Fig. 5.

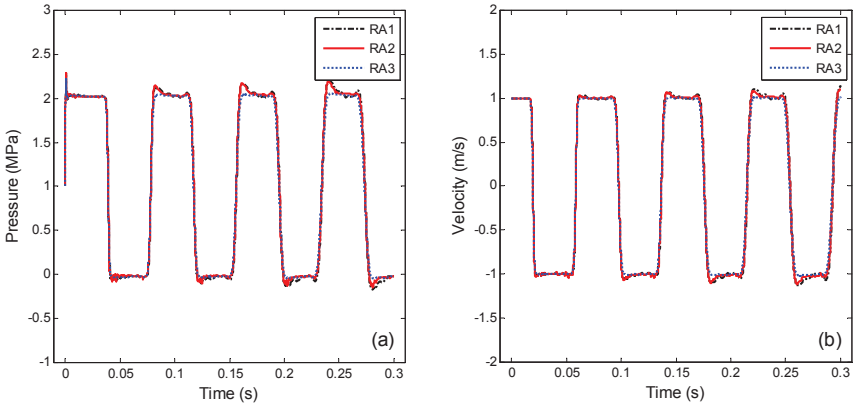

Figure 7: **Effect of random particle distribution on the (a) downstream pressure and (b) upstream velocity.**

To examine the effect of the other parameters, the uniform vertex-centered particle distribution (Fig. 2c) is used in the following sections.

5.2 Artificial viscosity

Artificial viscosity is modelled herein with the coefficients $\alpha = 1$ and $\beta = 2$ [20]. To demonstrate its effect, the problem is also simulated without artificial viscosity by setting the parameters α and β equal to zero. The results of these simulations are shown in Fig. 8. It clearly demonstrates that artificial viscosity suppresses numerical dispersion, which pollutes the solution in an unacceptable way.

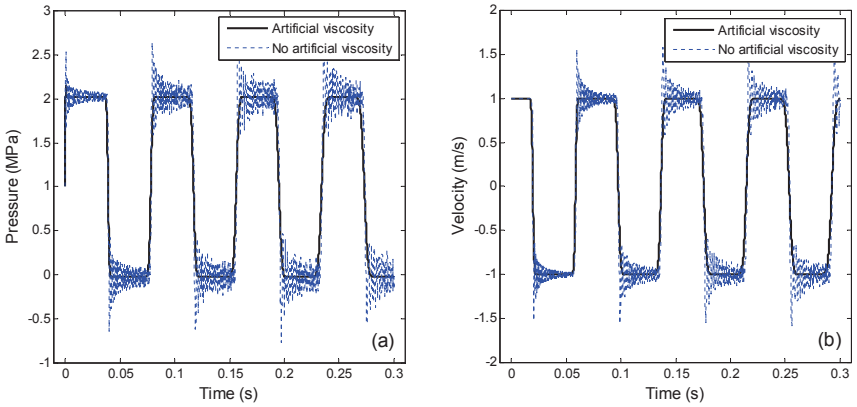

Figure 8: **Effect of artificial viscosity on the (a) downstream pressure and (b) upstream velocity.**

5.3 Pre-smoothing

Although the results of the present method match the MOC solution well, an overshoot at the first wave front is still visible in Fig. 4a. This overshoot can be removed by pre-smoothing. The pre-smoothing is applied to the velocity distribution in the first 5 time steps by using the smoothing features of the CSPM function approximation in (8). Then the derivative of the velocity is approximated from (9) with the smoothed velocity. This idea is from Monaghan [30] for the simulation of Riemann problems. The pre-smoothed CSPM results are depicted in Fig. 9. The overshoot is indeed diminished, but now a very small ($< 3\%$) offset is visible (Fig. 9a). This may be attributed to the numerical error of the CSPM function approximation in (8). The effect of pre-smoothing on the velocity is too small to be visible in Fig. 9b.

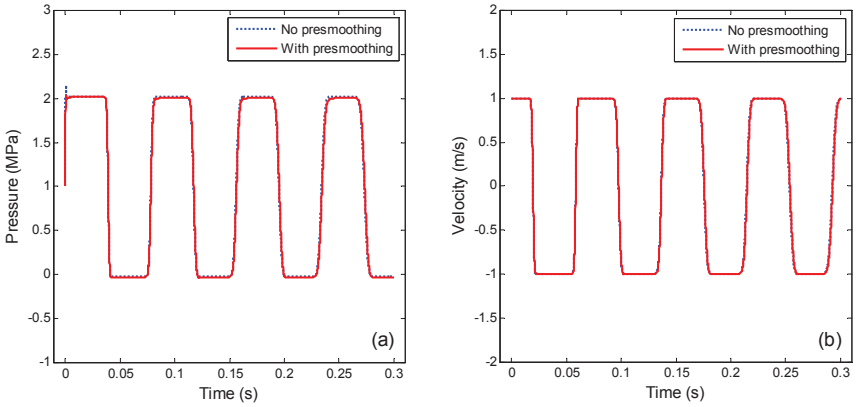

Figure 9: **Effect of pre-smoothing on the (a) downstream pressure and (b) upstream velocity.**

The velocity histories are in good agreement with the MOC solution. For this reason, the focus is only on the pressure histories in the following sections. Furthermore, friction is included ($\lambda = 0.02$), and used together with artificial viscosity and pre-smoothing.

5.4 Smoothing length

The two vital parameters in particle methods are the kernel W and the smoothing length h. For a given kernel, the smoothing length not only determines the numerical accuracy, but also affects the computational efficiency and numerical stability [23]. To avoid a singularity in (14) (see Subsection 4.2), the smoothing length must be $h > 0.5\Delta x$ (for evenly spaced particles).

Two effects of the smoothing length are observed. On one hand, smoothing lengths smaller than $1.0\Delta x$ result in dispersion errors as shown Fig. 10a. The smaller the smoothing length is, the more severe the numerical oscillations at the wave fronts become. The dispersion errors are minimized when h is close to $1.0\Delta x$. On the other hand, smoothing lengths larger than $1.0\Delta x$ result in numerical dissipation as shown in Fig. 10b. With increasing smoothing length, the dissipation or smearing effect is increasing, i.e. the wave fronts are less sharp and the amplitudes become smaller. This results in a big discrepancy between the CSPM calculations and the MOC solution.

In conclusion, for the transient flow problem investigated herein, a smoothing length h between $0.9\Delta x$ and $1.5\Delta x$ is sufficient to ensure non-singularity and

acceptable accuracy (minimal numerical dispersion and dissipation).

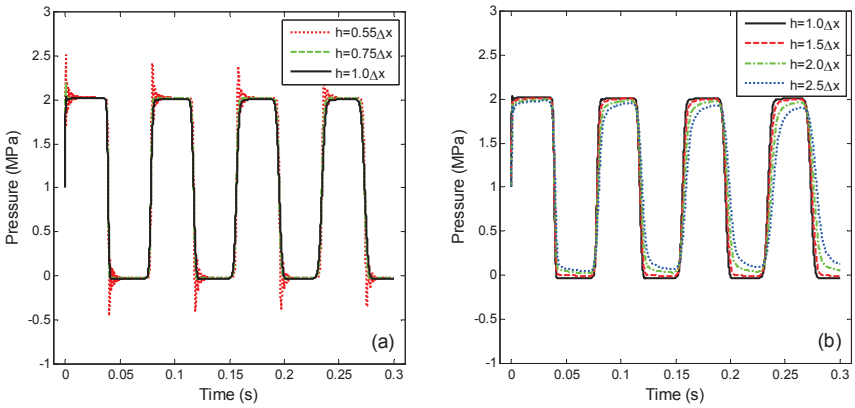

Figure 10: **Effect of the smoothing length on the downstream pressure with (a) small values and (b) large values.**

5.5 Number of particles

The effect of the number of particles on the CSPM calculations is exhibited in Fig. 11a for $h = 1.0\Delta x$. The effect mainly reveals as smearing. If only 21 particles are used, the first peak and period of the pressure history are predicted well, but the following peaks and amplitudes become less accurate. When more particles are employed, the smearing effect becomes less significant. Here, 201 particles are sufficient for acceptable accuracy.

5.6 Kernel function

Thus far the cubic spline kernel in (10) has been used. An alternative kernel is the modified Gaussian

$$W(q,h) := \frac{1.04823}{h\sqrt{\pi}} \begin{cases} e^{-q^2} - e^{-4}, & 0 \leqslant q < 2, \\ 0, & q \geqslant 2. \end{cases} \tag{18}$$

The comparison for the two kernels is depicted in Fig. 11b. Although both simulations predict the pressure history at the valve well, better results are obtained with the cubic spline kernel.

Many other kernels have been employed in meshfree methods [31]. The effect of the kernel not only depends on the specific meshfree method, but also on the specific problem. It is hard (if not impossible) to determine the optimum kernel, but the cubic spline function has proven its computational efficiency in SPH [20, 31] and it is most widely used in CSPM [21, 22, 28, 32].

6 TYPICAL WATERHAMMER RESULTS

The validity of CSPM for solving waterhammer problems is demonstrated in three test cases of practical importance.

6.1 Gradual valve closure

The test problem in Section 5 concerns travelling discontinuities generated by instantaneous valve closure. Such discontinuities pose problems to any numerical

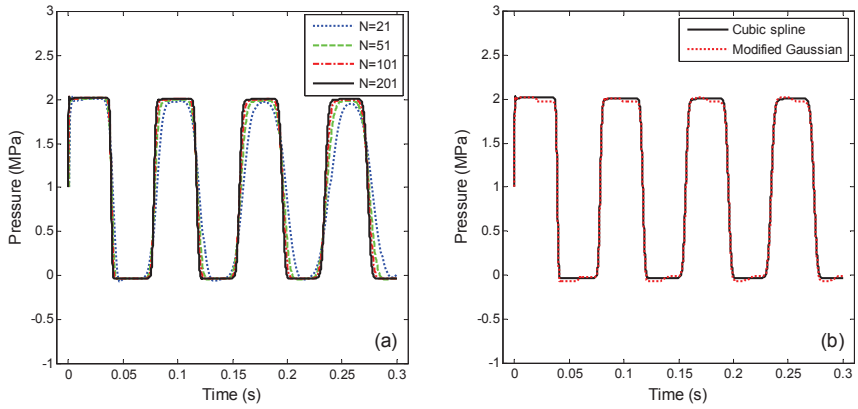

Figure 11: **Effect of the (a) number of particles and (b) kernel function on the downstream pressure.**

method. CSPM can deal with the discontinuities if a sufficient number of particles is taken (Fig. 12a), thereby noting that particle methods involve large numbers of particles anyway.

In practice these discontinuities do not occur, because the effective valve closure time has been larger than 10 ms in all reported work and pipe wall deformation causes dispersion of sharp wave fronts [33]. Figure 12b shows the pressure at the valve for gradual linear valve closure within 10 ms. The overshoot at the first pressure rise is absent, but artificial viscosity is still needed to suppress wiggles.

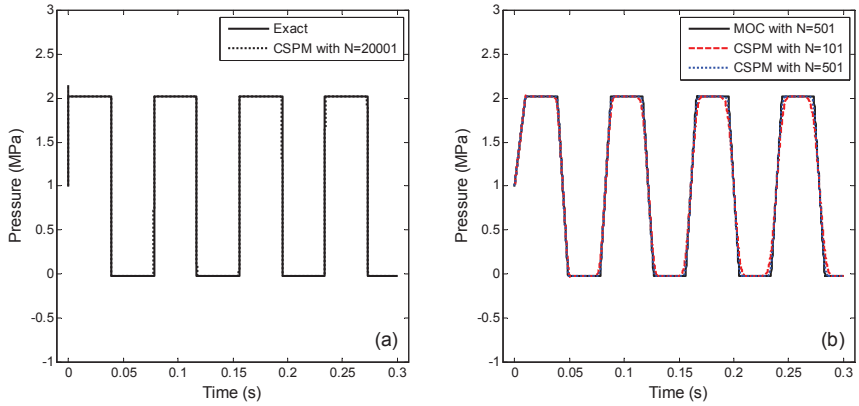

Figure 12: **Pressure history at valve. (a) Instantaneous valve closure and (b) gradual linear valve closure.**

6.2 Line pack

In long pipelines, the initial pressure gradient and skin friction lead to a phenomenon called line pack, where the pressure at the valve keeps rising once the valve is (suddenly) closed. The influence of friction is negligible in the results shown in Section 5, because the diameter of the pipe is large compared to its length. By taking a 100 times smaller diameter $D = 7.97$ mm and keeping the wave speed at 1025.7 m/s (through a thinner pipe wall) the results in Fig. 13a

are obtained for the same initial velocity $V_0 = 1.0$ m/s as in Section 5. Line pack is clearly visible and predicted well.

6.3 Column separation

Waterhammer not only involves high pressures, but also low pressures. If the absolute pressure at the valve drops to vapour pressure (0.02 bar for water at room temperature), the liquid column is separated from the valve by a vapour bubble (or vacuum). This phenomenon is called column separation. It can be modelled relatively simply by not allowing the pressure to drop below the vapour pressure. A constant (vapour) pressure boundary condition is then prescribed from which the downstream velocity of the elastic liquid column, and hence the cavity length, is calculated. The results obtained by CSPM are consistent with those by MOC, see Fig. 13b. The pressure spike at t = 0.12 s is physical and has been measured in laboratory test rigs [4]. It is the result of a mismatch of the water-hammer period $2L/c$ and the time of duration of the first column-separation [1]. The discrepancy between CSPM and MOC is attributed to the well-known sensitivity of the DVCM model used for column separation.

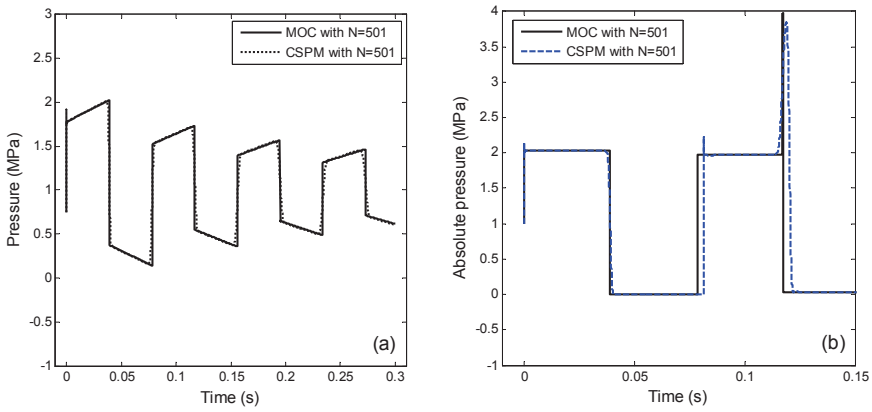

Figure 13: **Pressure history at valve. (a) Line pack and (b) column separation.**

7 CONCLUDING REMARKS

The corrective smoothed particle method (CSPM) is explored for fast transient flow in pipes. To solve the classical water-hammer equations, the time derivatives are approximated by the Euler forward method and the spatial derivatives by the corrective kernel estimate. The particles were assumed not to move. To suppress oscillations in the transient waves, a dissipative artificial viscosity term is added to the momentum equation. The CSPM results are in good agreement with conventional MOC solutions. The effect of parameters such as the particle distribution, artificial viscosity, smoothing function, smoothing length, pre-smoothing and number of particles has been investigated. The main conclusions are:

- Both uniform and random particle distributions can be used in CSPM. The vertex-centered particle distribution gives the best results.
- Artificial viscosity is indispensable in the numerical simulations of shocks and contact discontinuities to suppress unacceptable numerical oscillations.
- The pre-smoothing technique can be used to eliminate overshoots at sharp pressure wave fronts.

- The smoothing length has a significant effect on the CSPM results. When it is taken smaller than $0.9\Delta x$, CSPM suffers from dispersion errors (numerical oscillations). When it is taken larger than $1.5\Delta x$, dissipation errors (smearing) appear. In the range between $h = 0.9\Delta x$ and $h = 1.5\Delta x$, where Δx is the distance between particles, good results can be obtained.
- Although many other compactly supported functions can be used as the kernel in CSPM, the cubic spline kernel is the most efficient and accurate.
- Three typical water-hammer problems have been solved successfully with CSPM for the first time.

ACKNOWLEDGEMENT

The first author is grateful to the China Scholarship Council (CSC) for financially supporting his PhD studies.

APPENDIX: COMPUTATION STEPS

The flow chart for the simulation of transient pipe flow by CSPM is summarized as follows:

- Generate and distribute particles and define associated mass, density and smoothing lengths
- Loop over all particles:
  a) Search neighbour particles to establish interaction pairs;
  b) Calculate discretized kernel W_{ij} and its derivative $W_{ij,x}$.
- Assign initial pressures and velocities to particles
- Loop over all particles for time marching:
  1) Apply downstream boundary condition $V_N = 0$;
  2) Calculate $\frac{\partial V_i}{\partial x}$ by substituting V for f in (9) and obtain $\frac{DP_i}{Dt}$ from (13);
  3) Calculate the particle pressure according to (12);
  4) Apply upstream boundary condition $P_1 = P_{res}$;
  5) Calculate $\frac{\partial P_i}{\partial x}$ by substituting P for f in (9);
  6) Calculate the spatial derivative of the artificial viscosity from (14);
  7) Calculate the particle acceleration from (13);
  8) Compute the particle velocity according to (12).

References

(1) Wylie, E. B., Streeter, V. L. and Suo, L. S. (1993). Fluid Transients in Systems. Prentice-Hall: Englewood Cliffs.

(2) Lupton, H. R. (1953). Graphical analysis of pressure surges in pumping systems. Journal of the Institution of Water Engineers, 7: 87–125.

(3) Ghidaoui, M. S., Zhao, M., McInnis, D. A. and Axworthy, D. H. (2005). A review of water hammer theory and practice. Appl. Mech. Rev., 58(1): 49–76.

(4) Bergant, A., Simpson, A. R. and Tijsseling, A. S. (2006). Water hammer with column separation: A historical review. J. Fluid. Struct., 22: 135–171.

(5) Chaudhry, M. H. and Hussaini, M. Y. (1985). Second-order accurate explicit finite-difference schemes for waterhammer analysis. J. Fluid. Eng., 107: 523–529.

(6) Streeter, V. L. (1972). Unsteady flow calculation by a numerical method. Journal of Basic Engineering, 94: 457–466.

(7) Tan, J. K., Ng, K. C. and Nathan, G. K. (1987). Application of the centre implicit method for investigation of pressure transients in pipelines. Int. J. Numer. Meth. Fluids, 7(4): 395–406.

(8) Nathan, G. K., Tan, J. K. and Ng, K. C. (1988). Two-dimensional analysis of pressure transients in pipelines. Int. J. Numer. Meth. Fluids, 8(3): 339–349.

(9) Arfaie, M. and Anderson, A. (1991). Implicit finite-differences for unsteady pipe flow. Mathematical Engineering for Industry, 3: 133–151.

(10) Jović, V. (1995). Finite elements and the method of characteristics applied to water hammer modelling. Engineering Modelling, 8(3-4): 51–58.

(11) Shu, J. J. (2003). A finite element model and electronic analogue of pipeline pressure transients with frequency-dependent friction. J. Fluid. Eng., 125: 194–199.
(12) Guinot, V. (1998). Boundary condition treatment in 2 × 2 systems of propagation equations. Int. J. Numer. Meth. Eng., 42: 647–666.
(13) Hwang, Y. and Chung, N. (2002). A fast Godunov method for the water-hammer problem. Int. J. Numer. Meth. Fluids, 40(6): 799–819.
(14) Cheng, Y. G., Zhang, S. H. and Chen, J. Z. (1998). Water hammer simulation by the lattice Boltzmann method. Transactions of the Chinese Hydraulic Engineering Society, Journal of Hydraulic Engineering, 6: 25–31 (in Chinese).
(15) Cheng, Y. G. and Zhang, S. H. (2001). Numerical simulation of 2-D hydraulic transients using lattice Boltzmann method. Transactions of the Chinese Hydraulic Engineering Society, Journal of Hydraulic Engineering, 10: 32–37 (in Chinese).
(16) Wahba, E. M. (2006). Runge–Kutta time-stepping schemes with TVD central differencing for the water hammer equations. Int. J. Numer. Meth. Fluids, 52: 571–590.
(17) Sánchez Bribiesca, J. L. (1981). A finite-difference method to evaluate water hammer phenomena. J. Hydrol., 51: 305–311.
(18) Hou, Q., Zhang, L. X., Tijsseling, A. S. and Kruisbrink, A. C. H. (2012). Rapid filling of pipelines with the SPH particle method. Procedia Engineering, 31: 38–43.
(19) Hou, Q. (2012). Simulating Unsteady Conduit Flows with Smoothed Particle Hydrodynamics. PhD thesis, Eindhoven University of Technology.
(20) Liu, G. R. and Liu, M. B. (2003). Smoothed Particle Hydrodynamics: A Meshfree Particle Method. World Scientific, Singapore.
(21) Chen, J. K., Beraun, J. E. and Carney, T. C. (1999). A corrective smoothed particle method for boundary value problems in heat conduction. Int. J. Numer. Meth. Eng., 46: 231–252.
(22) Chen, J. K., Beraun, J. E. and Jih, C. J. (1999). An improvement for tensile instability in smoothed particle hydrodynamics. Comput. Mech., 23: 279–287.
(23) Monaghan, J. J. (2005). Smoothed particle hydrodynamics. Rep. Prog. Phys., 68: 1703–1759.
(24) Leveque, R. J. (2007). Finite Difference Methods for Ordinary and Partial Differential Equations: Steady-State and Time-Dependent Problems. SIAM, Philadelphia.
(25) Monaghan, J. J. and Gingold, R. A. (1983). Shock simulation by the particle method of SPH. J. Comp. Physics., 52: 374–381.
(26) Nguyen, V. P., Rabczuk, T., Bordas, S. and Duflot, M. (2008). Meshless methods: A review and computer implementation aspects. Math. Comput. Simulat., 79: 763–813.
(27) Tijsseling, A. S. (2003). Exact solution of linear hyperbolic four-equation systems in axial liquid-pipe vibration. J. Fluid. Struct., 18: 179–196.
(28) Chen, J. K., Beraun, J. E. and Jih, C. J. (2001). A corrective smoothed particle method for transient elastoplastic dynamics. Comput. Mech., 27: 177–187.
(29) Zhang, G. M. and Batra, R. C. (2004). Modified smoothed particle hydrodynamics method and its application to transient problems. Comput. Mech., 34: 137–146.
(30) Monaghan, J. J. (1997). SPH and Riemann solver. J. Comp. Physics., 136: 298–307.
(31) Fulk, D. A. and Quinn, D. W. (1996). An analysis of 1-D smoothed particle hydrodynamics kernels. J. Comp. Physics., 126: 165–180.
(32) Ostad, H. and Mohammadi, S. (2008). A field smoothing stabilization of particle methods in elastodynamics. Finite Elem. Anal. Des., 44: 564–579.
(33) Tijsseling, A. S., Lambert, M. F., Simpson, A. R., Stephens, M. L., Vítkovský, J. P. and Bergant, A. (2008). Skalak's extended theory of water hammer. J. Sound Vib., 310(3): 718–728.

PREVIOUS PUBLICATIONS IN THIS SERIES:

Number	Author(s)	Title	Month
12-10	W. Hundsdorfer A. Mozartova V. Savcenco	Monotonicity conditions for multirate and partitioned explicit Runge-Kutta schemes	May '12
12-11	J. Bogers K. Kumar P.H.L. Notten J.F.M. Oudenhoven I.S. Pop	A multiscale domain decomposition approach for chemical vapor deposition	May '12
12-12	K. Kumar T.L. van Noorden I.S. Pop	Upscaling of reactive flows in domains with moving oscillating boundaries	May '12
12-13	Q. Hou Y. Fan	Modified smoothed particle method and its application to transient heat conduction	May '12
12-14	Q. Hou A.C.H. Kruisbrink A.S. Tijsseling A. Keramat	Simulating water hammer with corrective smoothed particle method	May '12

Ontwerp: de Tantes,
Tobias Baanders, CWI